Crystal structure of GH43 exo-β-1,3-galactanase from the basidiomycete *Phanerochaete chrysosporium* provides insights into the mechanism of bypassing side chains

Kaori Matsuyama[1], Naomi Kishine[2], Zui Fujimoto[2], Naoki Sunagawa[1], Toshihisa Kotake[3], Yoichi Tsumuraya[3], Masahiro Samejima[1,4], Kiyohiko Igarashi[1,5*], and Satoshi Kaneko[6*]

1 Department of Biomaterial Sciences, Graduate School of Agricultural and Life Sciences, The University of Tokyo, 1-1-1 Yayoi, Bunkyo-ku, Tokyo 113-8657, Japan

2 Advanced Analysis Center, National Agriculture and Food Research Organization (NARO), 2-1-2 Kannondai, Tsukuba, Ibaraki 305-8518, Japan

3 Department of Biochemistry and Molecular Biology, Faculty of Science, Saitama University, 255 Shimo-Okubo, Sakura-ku, Saitama 338-8570, Japan

4 Faculty of Engineering, Shinshu University, 4-17-1, Wakasato, Nagano 380-8533, Japan

5 VTT Technical Research Centre of Finland, PO Box 1000, Tietotie 2, Espoo FI-02044 VTT, Finland

6 Department of Subtropical Bioscience and Biotechnology, Faculty of Agriculture, University of the Ryukyus, 1 Senbaru, Nishihara, Okinawa, 903-0213, Japan

* Corresponding author

KI: aquarius@mail.ecc.u-tokyo.ac.jp

SK: sakaneko@agr.u-ryukyu.ac.jp

Abbreviations (in order of appearance)

AGPs, arabinogalactan proteins; Gal, D-galactose; *Pc*1,3Gal43A, exo-β-1,3-galactanase from *Phanerochaete chrysosporium*; GH, glycoside hydrolase; GH43_sub24, GH family 43 subfamily 24; CBM, carbohydrate binding module; *Ct*1,3Gal43A, exo-β-1,3-galactanase from *Clostridium thermocellum*; BT3683, β-1,3-galactosidase from *Bacteroides thetaiotaomicron* VPI-5482; *Pc*Cel45A, endoglucanase V from *P. chrysosporium*; SeMet, selenomethionine; Gal3, β-1,3-galactotriose; WT, wild-type; WT_Gal, WT bound with Gal; E208Q_Gal3, E208Q bound with Gal3; E208A_Gal3, E208A bound with Gal3; *Pc*CBM35, CBM35 domain of *Pc*1,3Gal43A; Gal_{-1}, Gal residue occupied subsite -1; Gal_{+1}, Gal residue occupied subsite +1; Gal_{+2}, Gal residue occupied subsite +2; Gal2, β-1,3-galactobiose; Gal_site 1, the non-reducing terminal Gal residue of Gal3 bound to *Pc*CBM35; Gal_site 2, the middle Gal residue of Gal3 bound to *Pc*CBM35; Gal_site 3, the reducing terminal Gal residue of Gal3 bound to *Pc*CBM35; HPLC, high-performance liquid chromatography; *Pc*Lam55A, exo-β-1,3-glucanase from *P. chrysosporium*; SacteLam55A, GH55 exo-β-1,3-glucanase from *Streptomycs* sp.; *Hj*Cel3A, GH3 β-1,3-glucosidase from *Hypocrea jecorina*; Cte_2137, CBM35 of *C. thermocellum* cellulosomal protein; PEG, polyethylene glycol

Abstract (less than 250) (247)

Arabinogalactan proteins (AGPs) are functional plant proteoglycans, but their functions are largely unexplored, mainly because of the complexity of the sugar moieties, which are generally analyzed with the aid of glycoside hydrolases. In this study, we solved the apo and liganded structures of exo-β-1,3-galactanase from the basidiomycete *Phanerochaete chrysosporium* (*Pc*1,3Gal43A), which specifically cleaves AGPs. It is composed of a glycoside hydrolase family 43 subfamily 24 (GH43_sub24) catalytic domain together with a carbohydrate-binding module family (CBM) 35 binding domain. GH43_sub24 lacks the catalytic base Asp that is conserved among other GH43 subfamilies. Crystal structure and kinetic analyses indicated that the tautomerized imidic acid function of Gln263 serves instead as the catalytic base residue. *Pc*1,3Gal43A has three subsites that continue from the bottom of the catalytic pocket to the solvent. Subsite -1 contains a space that can accommodate the C-6 methylol of Gal, enabling the enzyme to bypass the β-1,6-linked galactan side chains of AGPs. Furthermore, the galactan-binding domain in CBM35 has a different ligand interaction mechanism from other sugar-binding CBM35s. Some of the residues involved in ligand recognition differ from those of galactomannan-binding CBM35, including substitution of Trp for Gly, which affects pyranose stacking, and substitution of Asn for Asp in the lower part of the binding pocket. *Pc*1,3Gal43A WT and its mutants at residues involved in substrate

recognition are expected to be useful tools for structural analysis of AGPs. Our findings should also be helpful in engineering designer enzymes for efficient utilization of various types of biomass.

63 **Running title**

64 Crystal structure of fungal GH43 galactanase

65

66 **Keywords (five from list + include less than 5)**

67 glycoside hydrolase family 43, carbohydrate binding module family 35 exo-β-1,3-galactanase,

68 arabinogalactan-protein, *Phanerochaete chrysosporium*

69

Introduction

Arabinogalactan proteins (AGPs) are proteoglycans characteristically localized in the plasma membrane, cell wall, and intercellular layer of higher land plants (1), in which they play functional roles in growth and development (2). The carbohydrate moiety of AGPs is composed of a β-1,3-D-galactan main chain and β-1,6-D-galactan side chain, decorated with arabinose, fucose, and glucuronic acid residues (1, 2). The chain lengths and frequencies of side chains are different among plant species, organs, and stages of development (3), and the overall structures of the carbohydrate moieties of AGPs are not yet fully understood.

Degradation of polysaccharides using specific enzymes is one approach to investigate their structures and roles. In this context, exo-β-1,3-galactanase (EC 3. 2. 1. 145) specifically cleaves the non-reducing end β-1,3-linked galactosyl linkage of β-1,3-galactans to release D-galactose (Gal). In particular, it releases β-1,6-galactooligosaccharides together with Gal from AGPs (4, 5), and is therefore useful for structural analysis of AGPs.

The basidiomycete *Phanerochaete chrysosporium* produces an exo-β-1,3-galactanase (*Pc*1,3Gal43A; GeneBank accession No. BAD98241) that degrades the carbohydrates of AGPs when grown with β-1,3-galactan as a carbon source (6). *Pc*1,3Gal43A consists of a glycoside hydrolase (GH) family 43 subfamily 24 (GH43_sub24) catalytic domain and a carbohydrate-binding module (CBM) belonging to family 35 (designated as *Pc*CBM6 in the previous paper) based on the amino acid sequences in the Carbohydrate-Active enZymes

(CAZy) database (http://www.cazy.org; 6-8). The properties of the enzyme have been analyzed using recombinant *Pc*1,3Gal43A expressed in the methylotrophic yeast *Pichia pastoris* (6). The CBM35 of *Pc*1,3Gal43A was characterized as the first β-1,3-galactan binding module, and *Pc*1,3Gal43A showed typical GH43_sub24 activity. The enzyme cleaves only β-1,3-linkages of oligosaccharides and polysaccharides, but produces β-1,6-galactooligosaccharides together with Gal. Thus, *Pc*1,3Gal43A specifically recognizes β-1,3-linked Gal, but can accommodate β-1,6-bound side chains (6).

Glycoside hydrolases are classified into families based on sequence similarity, while they are also divided into major two groups according to their catalytic mechanisms, i.e., inverting enzymes and retaining enzymes (9, 10). Inverting enzymes typically utilize two acidic residues that act as an acid and a base, respectively, and a hydroxyl group connected to anomeric carbon inverts from the glycosidic linkage after the reaction. GH43 enzymes are members of the inverting group, and share conserved Glu and Asp as the catalytic acid and base, respectively (8), but GH43_sub24 enzymes lack the catalytic base Asp (8, 11, 12). In *Ct*1,3Gal43A (from *Clostridium thermocellum*), Glu112 was thought to be the catalytic base (13), but in BT3683 (from *Bacteroides thetaiotamicron*), Glu367 (corresponding to Glu112 of *Ct*1,3Gal43A) was found not to act as a base, but to be involved in recognition of the C-4 hydroxyl group of the non-reducing terminal Gal, and instead, Gln577 is predicted to be the catalytic base in the form of an unusual tautomerized imidic acid (12). An example of GH

lacking a catalytic base, endoglucanase V from *P. chrysosporium* (*Pc*Cel45A), is already known, and based on the mechanism proposed for this enzyme, it is possible that tautomerized Gln functions as a base in GH43_sub24, or that this Gln stabilizes nucleophilic water. *Pc*Cel45A lacks the catalytic base Asp that is conserved in other GH45 subfamilies (14), but it uses the tautomerized imidic acid of Asn as the base, as indicated by neutron crystallography (15). However, it is difficult to understand the situation in GH43_sub24, since no holo structure with a ligand at the catalytic center has yet been solved in this family. Moreover, no structure of eukaryotic GH43_sub24 has yet been reported.

The CBM35 module is composed of approximately 140 amino acids. This family includes modules with various binding characteristics, and decorated with xylans, mannans, β-1,3-galactans, and glucans (16–21). The family members are divided into four clusters based on their sequences and binding specificities (17). The structures of CBM35s binding with xylan, mannan, and glucan have already been solved (16–21), but no structure of β-1,3-galactan-binding CBM35 has yet been reported.

In the present manuscript, we solved the apo and liganded structures of *Pc*1,3Gal43A. Based on the results, we discuss the catalytic mechanism and the mode of ligand binding to CBM35 in the two-domain structure.

Results

Overall structure of Pc*1,3Gal43A*

The crystal structure of the selenomethionine (SeMet) derivative of *Pc*1,3Gal43A was first determined by means of the multiwavelength anomalous dispersion method, and this was followed by structure determination of the ligand-free wild-type (WT), the WT bound with Gal (WT_Gal), the E208Q mutant co-crystallized with β-1,3-galactotriose (Gal3; E208Q_Gal3), and the E208A mutant co-crystallized with Gal3 (E208A_Gal3). Data collection statistics and structural refinement statistics are summarized in Tables 1 and 2, respectively.

The recombinant *Pc*1,3Gal43A molecule is composed of a single polypeptide chain of 428 amino acids (Gln21-Tyr448) with two extra amino acids, Glu19 and Phe20, derived from the restriction enzyme cleavage site, which are disordered and thus were not observed. The protein is decorated with *N*-glycans, since it was expressed in *Pichia* yeast. Up to three sugar chains are attached at Asn79, Asn194, and Asn389; the attached chains vary in position and structure, and most contain one or two *N*-acetylglucosamine moieties.

*Pc*1,3Gal43A is composed of two domains, and ligands introduced by soaking or co-crystallization are located in a subsite of the catalytic domain or the binding site of CBM35 (Fig. 1). The N-terminal catalytic domain consists of a five-bladed β-propeller (Gln21-Gly325), as in other GH clan-F enzymes, and the C-terminal domain (*Pc*CBM35)

takes a β-jellyroll fold (Thr326-Tyr448) structure, as in previously reported CBM35s (16–25). *Pc*CBM35 contains one calcium ion near the end of the first β-strand on a different domain surface from the plane to which the ligand binds (Fig. 1). The structure of *Pc*CBM35 is similar to those of other known CBM35s. The interface area is 686 A^2 and includes many water molecules. The PDBePISA server (http://www.ebi.ac.uk/msd-srv/prot_int/cgi-bin/piserver) indicates that the enzyme forms a complex in the crystal, but this is an effect of crystallization, and the enzyme exists as a monomer in solution (data not shown).

Sugar-binding structure of the Pc*1,3Gal43A catalytic domain*

The five-bladed β-propeller exhibits an almost spherical structure, and two central cavities are located at the ends of the pseudo-5-fold axis (Fig. 1). One of them contains the catalytic site and it is common in almost all GH43 enzymes. The catalytic site is located in the center of the five-bladed β-propeller, whose blades are formed by Gln21 or Asn22-Leu87 (I in Fig. 1), Ser88-Asp155 (II in Fig. 1), Ser156-Gly204 (III in Fig. 1), Ala205-Ser247 (IV in Fig. 1), and Ala248-Asp297 (V in Fig. 1).

As shown in Fig. 2, the Gal3 molecule co-crystallized with the E208Q mutant occupies subsites -1, +1, and +2 of the catalytic site, from the non-reducing end to the reducing end. Gal_{-1} is located at the bottom of the catalytic cavity, and Gal_{+1} and Gal_{+2} extend linearly

outwards. Gal_{+1} is half buried in the cavity, whereas Gal_{+2} is exposed at the surface (Fig. 2A).

Gal_{-1} adopts a $^{1}S_{3}$ skew boat conformation and interacts with many residues via hydrogen bonds and hydrophobic interactions. As shown in Fig. 2B and C, the C-2 hydroxyl group of Gal_{-1} forms hydrogen bonds with NH_2 of Arg103 and with OE1 of Gln263 via water. In addition, this water molecule is bound with O of Gly228. The C-3 hydroxyl group of Gal_{-1} also forms a hydrogen bond with OE2 of Glu57 via water. Glu102, Tyr126, Asp158, Gln208, Thr226, Trp229, and Gln263 interact with Gal3 through hydrophobic interactions. Notably, Trp229 supports the flat C3-C4-C5-C6 structure of Gal_{-1}, and Tyr126 recognizes the C-6 methylol and C-4 hydroxyl groups, while Glu102 recognizes the C-3 hydroxyl and C-4 hydroxyl groups. In Gal_{+1} (as shown in Fig. 2B and C), the C-2 hydroxyl group forms a hydrogen bond with NE2 of Gln208 and N of Gly228, while O5 forms a hydrogen bond with ND2 of Asn180, and C-6 hydroxyl group forms a hydrogen bond with OD1 of Asn179 via water. Tyr126, Arg157, Asn180, and Gln208 interact hydrophobically with Gal. In Gal_{+2} (Fig. 2B and C), the C-2 and C-4 hydroxyl groups form hydrogen bonds with OG1 of Thr226 and ND2 of Asn180, respectively. In addition, Thr226 interacts with Gal_{+2} through hydrophobic interaction. Furthermore, the glycosidic oxygen between Gal_{+1} and Gal_{+2} interacts with ND2 of Asn180 through a hydrogen bond.

In the structure of WT_Gal, one Gal was found at subsite -1, taking a $^{4}C_{1}$ chair conformation with α-anomeric conformation of the C-1 hydroxyl group (data not shown). The

183 binding mode of Gal_{-1} is almost the same as that in E208Q_Gal3, but the C-1 hydroxyl group
184 in the axial position forms hydrogen bonds with Gly228 and Gln263. No Gal3 molecule was
185 observed at the catalytic domain in the structure of the Gal3 co-crystallized E208A mutant.
186 In order to identify the catalytic residues, we examined the relative activity of WT
187 and the six mutants towards β-1,3-galactobiose (Gal2) and Gal3. WT showed 5.58±0.35 and
188 11.15±0.39 units of activity (μmol Gal /min/nmol enzyme) towards Gal2 and Gal3,
189 respectively, whereas the six mutants showed no detectable activity (Fig. S1), suggesting that
190 these residues are all essential for the catalysis.
191
192 *Sugar-binding structure of CBM35 in* Pc*1,3Gal43A*
193 *Pc*1,3Gal43A has one CBM35 domain at the C-terminus. We previously reported that this
194 enzyme has a CBM6-like domain (6), but it has been reclassified into the CBM35 family (7).
195 The β-jellyroll fold domain is accompanied by a single calcium ion binding site on a different
196 domain surface than the surface to which the ligand at the end of the first β chain binds, and
197 this corresponds to a conserved calcium ion binding site in CBM35s. Some CBM35 modules
198 bind another calcium ion at a site at the top of domain (16), but *Pc*CBM35 lacks this second
199 calcium ion binding site (Fig. 1).
200 In E208A_Gal3, electron density of Gal3 was observed in the ligand binding site of
201 *Pc*CBM35. As illustrated in Fig. 3A and S2, 2Fo-Fc omit maps showed that the binding mode

of *Pc*CBM35 with ligands is “exo-type”, corresponding to type-C CBM (26). The asymmetric unit of E208A_Gal3 contained four *Pc*1,3Gal43A molecules and each molecule binds to the non-reducing end of Gal3 (called Gal_site 1), as in other CBM35 modules. However, the middle Gal (Gal_site 2) and the reducing end Gal (Gal_site 3) are found in two main locations (Fig. 3), though residues involved in the interactions with the ligand in each molecule were mostly shared. The Gal_site 1 forms hydrogen bonds with Tyr355 and Arg388 and interacts hydrophobically with Leu342, Gly354, Tyr438, and Asp441. The Gal_site 2 interacts hydrophobically with Gly383 and Asp384. The main ligand interaction in the Gal_site 3 involves Gly409 and Gly410, but in addition to these residues, Asn411 is also involved in ligand recognition in chain C (Fig. 4).

Ensemble refinement

In order to understand the fluctuation of ligands, ensemble refinements were performed with the refined models. This method produces ensemble models by employing the combination of X-ray structure refinement and molecular dynamics. These models can simultaneously account for anisotropic and anharmonic distributions (27). Four different pTLS values (%) of 0.6, 0.8, 0.9, and 1.0 were set for each model. Table 3 shows the statistical scores of the refinement with the most appropriate pTLS value for each model. Focused views of the catalytic site in the catalytic domain and the ligand binding site of the CBM are shown in Fig.

221 5 and 6, respectively. Note that structures containing multiple molecules in the asymmetric
222 unit (WT and E208A_Gal3) are found for all molecules in this paper.

223 In the catalytic site, the vibration levels of some residues were significantly different
224 between the apo and holo forms. As shown in Fig. 5, Tyr126, Arg157, Asp158, Asn179,
225 Asn180, Gln181, Trp229, and Gln263 in the liganded structures (Fig. 5B, C, F, G, J, and K)
226 showed smaller vibrations than in the apo structures (Fig. 5A, D, E, H, I, and L). These results
227 indicate that side chain fluctuations converge upon ligand binding. Comparison of the
228 Gal-bond structure (i. e. WT_Gal; Fig. 5B, F, J) with the Gal3-bond structure (i. e.
229 E208Q_Gal3; Fig. 5 C, G, K) showed that the fluctuations of Glu(Gln)208, Asn179, and
230 Thr226 of E208Q_Gal3 were smaller than these in WT_Gal. Therefore, it can be inferred that
231 these residues recognize the ligands at the plus subsites. The catalytic acid, Glu208, has two
232 major conformations in WT and WT_Gal. These two conformations were also reported in the
233 BT3683 structure (12). Thus, the movement of this residue appears to be important for
234 catalysis. Gln263 shows one conformation (Fig. 5A-D) that is identical to the result of the
235 ensemble refinement of Asn92, known as imidic acid in *Pc*Cel45A (Fig. S3). Glu102 may
236 distinguish non-reducing terminal Gal, since it interacts with the axial C-4 hydroxyl group of
237 Gal_{-1} (12). The vibration degree of Glu102 was different between WTs and mutants, so its
238 conformation does not depend on the ligand localization, but reflects interaction with Glu208,
239 which serves as a general acid. Asp158 of WT and E208A_Gal3 show greater vibration than

WT_Gal and E208Q_Gal3. The role of Asp158 is thought to be a pKa modulator, therefore its function and conformational stability might be related. Focusing on Fig. 5I-L, there were large differences in the fluctuation level of Trp229. E208Q_Gal3 (Fig. 5K) showed small movements of Trp229, but other structures showed much larger fluctuations (Fig. 5I, J, L). These results suggest that this Trp is normally flipped and forms a π-π interaction to anchor the ligand in the proper position upon arrival. A histogram of the dihedral angle is shown in Fig. S4.

As regards the ligand binding site of the CBM, a comparison of each chain of the E208A_Gal3 asymmetric unit showed no significant difference in the vibration levels of each residue involved in ligand binding (Fig. 6). However, ensemble refinement revealed that Gal_site 1 and Gal_site 2 do not show huge fluctuations, while Gal_site 3 has many conformations. They include the same conformation of each chain Gal of X-ray crystallography. Interestingly, a spatial difference in fluctuations was observed between ligands bound to the catalytic site and to the ligand binding site of CBM35 (Fig. 7). At the catalytic site, Gal_{-1} is anchored in the appropriate position, and Gal_{+2} appears to fluctuate in a planar fashion as it interacts with the surrounding residues. In the CBM, it was inferred that Gal_site 1 is fixed and Gal_site 3 is adsorbed at the appropriate location at the binding site while fluctuating in three dimensions.

Discussion

Most exo-β-1,3-galactanases belonging to GH43_sub24 possess CBMs that can be classified into CBM35 or CBM13 (8). In this study, we elucidated the structure of a β-1,3-galactan binding module for the first time by solving the structure of a GH43_sub24 containing CBM35, and obtained the ligand-bound structures of both the catalytic and sugar binding domains of *Pc*1,3Gal43A. This is also the first study to reveal the structure of a eukaryotic exo-β-1,3-galactanase. This information will be useful to understand how the CBM35 module interacts with β-1,3-galactan in combination with the GH43_sub24 catalytic module.

How does Pc*1,3Gal43A hydrolyze β-1,3-galactan?*

Although catalytic residues such as Glu and Asp are conserved in GH43 as a catalytic acid and base, respectively, GH43_sub24 lacks such a base residue. Mewis and co-workers suggested that GH43_sub24 may use Gln in the base role via conversion to imidic acid, or use an exogenous base, or utilize the Grotthuss mechanism of catalysis (8, 12). In this study, we measured the enzyme activity of six variants of the three residues speculated to be involved in the catalytic reaction. As shown in Fig. S1, production of Gal by the mutants was not detected by means of high-performance liquid chromatography (HPLC) analysis, suggesting that all three residues are essential for the catalytic activity of *Pc*1,3Gal43A. Glu102, Glu208, and Gln263 are speculated to serve in C-4 hydroxyl group recognition, as a catalytic acid, and as a

277 catalytic base, respectively. These residues are well conserved in GH43_sub24, as shown in
278 Fig. S5.

279 In GH43_sub24, only bacterial enzyme structures have been solved so far
280 (http://www.cazy.org/GH43_24.html). In order to understand the catalytic mechanism of
281 *Pc*1,3Gal43A, we compared its structure with those of BT3683 and *Ct*1,3Gal43A (Fig. 8).
282 Most of the residues that interact with ligands are conserved in these three enzymes. In subsite
283 -1, all residues, Glu57, Glu102, Arg103, Tyr126, Asp158, Glu208, Trp229, and Gln263, of
284 *Pc*1,3Gal43A are conserved, indicating that the binding mode at subsite -1 is fully conserved
285 in GH43_sub24. Based on the results of ensemble refinement, Trp229 showed huge
286 fluctuation, especially in the apo structure (Fig. 5I-L). Trp541 of BT3683, which corresponds
287 to Trp229 of *Pc*1,3Gal43A, has a polar interaction with Gal (12). Trp229 fluctuates in solution
288 and plays a role in holding the substrate at the catalytic site through polar interactions. On the
289 other hand, Asn179 and Thr226 of *Pc*1,3Gal43A are replaced by Asp490 and Cys538 in
290 BT3683 and by Glu199 and Cys247 in *Ct*1,3Gal43A. Since all of these enzymes can
291 accommodate a β-1,6-branched side chain (6, 12, 28), we considered that these residues are
292 not related the mechanism of side-chain accommodation.

293 The bypass mechanism of *Pc*1,3Gal43A, which enables accommodation of the
294 β-1,6-galactan side-chain so that the β-1,3-galactan main chain can be cleaved, appears to
295 depend on the orientation of the C-6 methylol group of Gal3 at each subsite. The C-6

296 methylol group of Gal_{-1} is exposed to the solvent, so that the side chain can be accommodated
297 externally. The C-6 methylol groups of Gal_{+1} and Gal_{+2} are also exposed to the solvent, so that
298 the enzyme should be able to cleave the β-1,3-linkage of continuously β-1,6-substituted
299 galactan, and a similar situation has been reported for BT3683 (12). Moreover, there are
300 spaces near the non-reducing terminal Gal in these enzymes (12, 29). This enables the
301 enzymes to degrade the main chain, even if the side chain contains multiple carbohydrates.
302 Similarly, β-1,3-glucanases belonging to GH55 also bypass the β-1,6-glucan side chain and
303 degrade β-1,3-glucan from the non-reducing end (29, 30). Comparing the surface structure of
304 the catalytic site of *Pc*1,3Gal43A with that of these GH55 exo-β-1,3-glucanase from *P.*
305 *chrysosporium* (*Pc*Lam55A), we see that *Pc*1,3Gal43A has a small pocket-like space capable
306 of accepting the C-6 side chain of Gal at subsite -1 (Fig. 9A and B). In addition, the C-6
307 methylol group of Gals, located at the positive subsites of *Pc*1,3Gal43A, are exposed to
308 solvent in a similar manner to that reported for SacteLam55A, GH55 exo-β-1,3-glucanase
309 from *Streptomyces* sp. SirexAA-E (Fig. 9A and C). Structures capable of accepting
310 non-reducing terminal Gal with β-1,6-linked Gal are conserved among GH43_sub24 of
311 known structure (Fig. 8 and S5). In the non-bypassing GH3 *Hypocrea jecorina* β-glucosidase
312 (*Hj*Cel3A), the C-6 hydroxyl group of non-reducing glucose is oriented toward the enzyme,
313 introducing steric hindrance (Fig. 9D; 31). In other words, enzymes bypassing side chains
314 have a space adjacent to C-6 of the non-reducing terminal sugar, and the positive subsites are

315 particularly wide, allowing side chains of the substrate to be accommodated. In contrast,
316 enzymes unable to bypass the side chain have no space next to the -1 subsite and have a
317 narrow entrance to the catalytic site, so that they are unable to accommodate side chains (Fig.
318 9D).

319 Although the electron density of Gal3 was observed in the present study,
320 *Pc*1,3Gal43A is proposed to have four subsites ranging from -1 to +3, based on biochemical
321 experiments (6). As mentioned above, although *Pc*1,3Gal43A has a structure capable of
322 accepting the C-6 side chain, its degradation activity towards β-1,3/1,6-galactan is only
323 approximately one-fifth that of the linear β-1,3-galactan (6). This difference in reactivity may
324 be due to the structure of the sugar. The β-1,3-galactan in solution has a right-handed triple
325 helical structure with 6 to 8 Gal residues per turn (32, 33), with the C-6 methylol group
326 pointing outward to avoid collisions between the β-1,6-bonded Gal side chains (32). However,
327 as shown in Fig. S6, Gal3 bound to the catalytic site of *Pc*1,3Gal43A is anchored to the
328 enzyme, so that the helix of the glycans differs from the usual state in solution. Therefore, the
329 reason why the hydrolytic activity of *Pc*1,3Gal43A towards β-1,3/1,6-galactan is lower than
330 that towards β-1,3-galactan may be interference between the β-1,6-Gal(s) side chains as a
331 result of changes in the helical state of the main chain.

332

333 *How does* Pc*CBM35 recognize β-1,3-galactan?*

Although the amino acid sequence similarity of CBM35s is not so high, important residues involved in ligand binding are well conserved (17). The modules belonging to CBM35 can be divided into four clades according to the mode of ligand binding, and the diversity in ligand binding and in the calcium ion-coordinating residue account for the various ligand binding specificities (17, Fig. 10A). Moreover, the residues involved in ligand binding of *Pc*CBM35 differ from those of CBM35, which binds to α-Gal of galactomannan. This CBM is one part of a protein predicted to be the β-xylosidase of *C. thermocellum* cellulosomal protein (Cte_2137; Fig. 10), which belongs to the same cluster as *Pc*CBM35 (17). There are some differences between the residues interacting with α-Gal of Cte_2137 and those interacting with β-Gal of *Pc*CBM35. For instance, the regions of Ala352 to Tyr355 and Tyr438 to Asp441 of *Pc*CBM35 correspond to Val39 to Gly42 and Ser136 to Asn140 of Cte_2137, which are related to ligand specificity (Fig. 10). Especially, Asn140 of Cte_2137 is not conserved but replaced Asp441 in *Pc*CBM35 and is located at the bottom of the ligand binding site. Furthermore, Trp108 of Cte_2137, which is conserved in *Pc*CBM35, plays a key role in stacking the pyranose ring (17), while in CBM35 of *Pc*1,3Gal43A, this Trp residue is replaced with Gly (Fig. 10B). In other words, although *Pc*CBM35 and Cte_2137 are in the same cluster, the residues involved in ligand recognition are different, and this difference affects the discrimination between β-Gal and α-Gal, and between galactan and galactomannan. It is still unclear how CBM35s acquire such variation of binding specificity within a similar binding

353 architecture. However, a detailed understanding of the molecular mechanisms of
354 polysaccharide recognition by CBM35 will be essential for efficient utilization of various
355 types of biomass.

356 In conclusion, we have determined the crystal structure of the catalytic and binding
357 domains of *Pc*1,3Gal43A with the aim of reaching a detailed understanding of the mechanism
358 of substrate accommodation by side-chain-bypassing galactanase. *Pc*1,3Gal43A uses Glu as
359 the catalytic acid and Gln as the catalytic base, and has a structure in which the side chain of
360 the substrate does not interfere with the catalytic reaction, thus making it possible to degrade
361 the β-1,3-galactan main chain of AGPs despite the presence of the β-1,6-galactan side chain.
362 Thus, although polysaccharides have a variety of molecular decorations, it appears that the
363 structures of the degrading enzymes enable them to recognize specific features of the
364 substrate while accommodating the variations. The introduction of mutations in substrate
365 recognition residues to create enzymes with altered substrate recognition properties is
366 expected to be helpful in the structural analysis of AGP glycans and also for the preparation of
367 useful oligosaccharides.

Experimental procedures

Expression of Pc*1,3Gal43A and its mutants*

The E208Q, E208A, E102Q, E102A, Q263E, and Q263A mutants were constructed by inverse PCR using PrimeSTAR MAX (Takara, Tokyo, Japan). For crystallization, *Pc*1,3Gal43A WT, E208Q, and E208A from *P. chrysosporium* were expressed in *P. pastoris* and purified as previously reported (7). For reactivity assay, WT and mutants were purified by using SkillPak TOYOPEARL Phenyl-650M (c.v. = 5 ml, Tosoh, Tokyo, Japan) equilibrated with 20 mM sodium acetate buffer, pH 4.0, containing 1 M ammonium sulfate, and the enzymes were eluted with 20 mM sodium acetate buffer, pH 4.0, containing 0.7 M ammonium sulfate. SeMet-labeled *Pc*1,3Gal43A was expressed as previously reported (7).

Preparation for β-1,3-galactooligosaccharides and crystallization of Pc*1,3Gal43A*

Gal2 and Gal3 were prepared as previously reported (6). The protein solution was concentrated to A_{280} of 10 ~ 15 and used for the crystallization setup. The WT plate crystal used for data collection was obtained from a reservoir of 2.1 M ammonium sulfate, 0.1 M citrate buffer, pH 5.5. Other WT crystals were obtained from solutions in 16 % (w/v) polyethylene glycol (PEG) 10000, 0.1 M ammonium sulfate, 0.1 M bis-tris, pH 5.5, and 5.0 % (v/v) glycerol. SeMet crystals were obtained from 16 % (w/v) PEG 10000, 95 mM ammonium sulfate, 95 mM bis-tris, pH 5.5, and 4.8 % (v/v) glycerol. Two types of crystals,

thin plate crystals (space group $P2_1$) and rod crystals ($P2_12_12_1$) appeared under the same condition. Cocrystallization of the E208Q mutant with 10 mM Gal3 in 16 % (w/v) PEG 10000, 95 mM ammonium sulfate, 95 mM bis-tris, pH 5.5, and 4.8 % (v/v) glycerol afforded thin plate crystals. The E208A mutant was cocrystallized with 10 mM Gal3 in 0.2 M potassium nitrate, 15% (w/v) PEG 6000, 20 mM sodium citrate, pH 4.5, and 5 % glycerol to afford bipyramidal crystals.

Data collection and structure determination

Diffraction experiments for *Pc1,3Gal43A* crystals were conducted at the beamlines of the Photon Factory (PF) or Photon Factory Advanced Ring (PF-AR), High Energy Accelerator Research Organization, Tsukuba, Japan (Table 1). Diffraction data were collected using CCD detectors (Area Detector Systems Corp., Poway, CA, USA). Crystals were cryocooled in a nitrogen gas stream to 95 K. For data collection of the WT enzyme complexed with Gal3, *Pc*1,3Gal43A crystals were soaked in a drop containing 1 % (w/v) Gal3 for 10 min before the diffraction experiment. The data were integrated and scaled using the programs DENZO and SCALEPACK in the HKL2000 program suite (34)

Crystal structure was determined by means of the multiwavelength anomalous dispersion method using a SeMet-labeled crystal (7). Initial phases were calculated using the SOLVE/RESOLVE program (35) from five selenium atom positions. The resultant

406 coordinates were subjected to the auto-modeling ARP/wARP program (36) in the CCP4
407 program suite (37), and manual model building and molecular refinement were performed
408 using Coot (version 0.8.9, University of Oxford, Oxfordshire, England; 46), REFMAC5
409 (version 7.0.063, Science & Technology Facilities Council, England; 47), phenix.refine (40),
410 and phenix.ensemble_refinement (27, 41, 42) in the Phenix suite of programs (version
411 1.13-2998-000, Lawrence Berkeley National Laboratory, USA; 51). The refinement statistics
412 are summarized in Table 2.

413 For the analyses of WT, and ligand bound structures, structural determination was
414 conducted by the molecular replacement method with the MolRep program (44) in the CCP4
415 program suite using the SeMet or ligand-free structure as the starting model. Bound sugars,
416 water molecules and crystallization agents were modelled into the observed electron density
417 difference maps. Calcium ion was modelled based on the electron density map and the
418 coordination distances. Three N-glycans were observed, and the identified sugars were
419 modelled. The stereochemistry of the models was analyzed with LigPlot + (version 1.4.5; 53,
420 54) and structural drawings were prepared using PyMOL (version 2.2.3, Schrödinger, LLC).
421 The atomic coordinates and structure factors (codes 7BYS, 7BYT, 7BYV, and 7BYX) have
422 been deposited in the Protein Data Bank (http://wwpdb.org/).

423

424 *Enzymatic activity assay of* Pc*1,3Gal43A and its mutants*

To evaluate the reactivity towards Gal2 and Gal3 of WT and each mutant, 20 nM enzyme was incubated with 0.263 or 0.266 mM galactooligosaccharides in 20 mM sodium acetate, pH 5.0, for 30 min at 30 ℃, respectively. The reaction was stopped by heating at 95 ℃ for 5 min. The supernatant was separated with 75% (v/v) acetonitrile on a Shodex Asahipak NH2P-50 4E column (Showa Denko, Tokyo, Japan), and the amount of released Gal was determined by HPLC (LC-2000 series; Jasco, Tokyo, Japan) with a Corona charged aerosol detector (ESA Biosciences, now Thermo Fisher Scientific Corporation, Massachusetts, USA). One unit of enzyme activity was defined as the amount of enzyme that releases 1 μmol of Gal per one minute per one nmol of enzyme under our experimental conditions.

Acknowledgments

We would like to thank Dr. Takuya Ishida (Japan Aerospace Exploration Agency) for helping with the crystallization and structure refinement. We also thank the staff of Photon Factory for X-ray data collection.

Author contributions

K. M., N. K., and Z.F. solved and refined structures; K.M. and N. S. assayed enzymatic activity; T. K. and Y. T. prepared galactooligosaccharides (Gal2 and Gal3); K. M., M. S, K. I, and S.K. wrote the manuscript, and all authors commented on the manuscript.

Funding and additional information

This research was partially supported by a Grant-in-Aid for Scientific Research (B) 19H03013 to K.I.) from the Japan Society for the Promotion of Science (JSPS) and a Grant-in-Aid for Innovative Areas from the Japanese Ministry of Education, Culture, Sports, and Technology (MEXT) (No. 18H05494 to K.I.). In addition, K.I. thanks Business Finland (BF, formerly the Finnish Funding Agency for Innovation (TEKES)) for support via the Finland Distinguished Professor (FiDiPro) Program "Advanced approaches for enzymatic biomass utilization and modification (BioAD)".

Conflict of interest

The authors declare no conflicts of interest associated with this manuscript.

References

1. Tsumuraya, Y., Hashimoto, Y., Yamamoto, S., and Shibuya, N. (1984) Structure of L-arabino-D-galactan-containing glycoproteins from radish leaves. *Carbohydr. Res.* **134**, 215–228

2. Majewska-Sawka, A., and Nothnagel, E. A. (2000) The Multiple Roles of Arabinogalactan Proteins in Plant Development. *Plant Physiol.* **122**, 3–9

3. Ellis, M., Egelund, J., Schultz, C. J., and Bacic, A. (2010) Arabinogalactan-proteins: Key regulators at the cell surface? *Plant Physiol.* **153**, 403–419

4. Tsumuraya, Y., Nobuyuki, M., Yohichi, H., and Kováč, P. (1990) Purification of an Exo-β-(1-3)-D-galactanase of *Irpex lacteus* (*Polyporus tulipiferae*) and its action on arabinogalactan-proteins. *J. Biol. Chem.* **265**, 7207–7215

5. Pellerin, P., and Brillouet, J. M. (1994) Purification and properties of an exo-(1→3)-β-D-galactanase from Aspergillus niger. *Carbohydr. Res.* **264**, 281–291

6. Ichinose, H., Yoshida, M., Kotake, T., Kuno, A., Igarashi, K., Tsumuraya, Y., Samejima, M., Hirabayashi, J., Kobayashi, H., and Kaneko, S. (2005) An exo-β-1,3-galactanase having a novel β-1,3-galactan-binding module from *Phanerochaete chrysosporium*. *J. Biol. Chem.* **280**, 25820–25829

7. Ishida, T., Fujimoto, Z., Ichinose, H., Igarashi, K., Kaneko, S., and Samejima, M. (2009) Crystallization of selenomethionyl exo-β-1,3-galactanase from the

basidiomycete *Phanerochaete chrysosporium*. *Acta Crystallogr. Sect. F Struct. Biol. Cryst. Commun.* **65**, 1274–1276

8. Mewis, K., Lenfant, N., Lombard, V., and Henrissat, B. (2016) Dividing the large glycoside hydrolase family 43 into subfamilies: A motivation for detailed enzyme characterization. *Appl. Environ. Microbiol.* **82**, 1686–1692

9. Davies, G., and Henrissat, B. (1995) Structures and mechanisms of glycosyl hydrolases. *Structure*. **3**, 853–859

10. Rye, C. S., and Withers, S. G. (2000) Glycosidase mechanisms. *Curr. Opin. Chem. Biol.* **4**, 573–580

11. Cartmell, A., McKee, L. S., Pena, M. J., Larsbrink, J., Brumer, H., Kaneko, S., Ichinose, H., Lewis, R. J., Viksø-Nielsen, A., Gilbert, H. J., and Marles-Wright, J. (2011) The structure and function of an arabinan-specific α-1,2-arabinofuranosidase identified from screening the activities of bacterial GH43 glycoside hydrolases. *J. Biol. Chem.* **286**, 15483–15495

12. Cartmell, A., Muñoz-Muñoz, J., Briggs, J. A., Ndeh, D. A., Lowe, E. C., Baslé, A., Terrapon, N., Stott, K., Heunis, T., Gray, J., Yu, L., Dupree, P., Fernandes, P. Z., Shah, S., Williams, S. J., Labourel, A., Trost, M., Henrissat, B., and Gilbert, H. J. (2018) A surface endogalactanase in *Bacteroides thetaiotaomicron* confers keystone status for arabinogalactan degradation. *Nat. Microbiol.* **3**, 1314–1326

13. Jiang, D., Fan, J., Wang, X., Zhao, Y., Huang, B., Liu, J., and Zhang, X. C. (2012) Crystal structure of 1,3Gal43A, an exo-β-1,3-galactanase from *Clostridium thermocellum*. *J. Struct. Biol.* **180**, 447–457

14. Igarashi, K., Ishida, T., Hori, C., and Samejima, M. (2008) Characterization of an endoglucanase belonging to a new subfamily of glycoside hydrolase family 45 of the basidiomycete *Phanerochaete chrysosporium*. *Appl. Environ. Microbiol.* **74**, 5628–5634

15. Nakamura, A., Ishida, T., Kusaka, K., Yamada, T., Fushinobu, S., Tanaka, I., Kaneko, S., Ohta, K., Tanaka, H., Inaka, K., Higuchi, Y., Niimura, N., Samejima, M., and Igarashi, K. (2015) " Newton's cradle " proton relay with amide – imidic acid tautomerization in inverting cellulase visualized by neutron crystallography. *Sci. Adv.* **1:e1500263**, 1–7

16. Montanier, C., Van Bueren, A. L., Dumon, C., Flint, J. E., Correia, M. A., Prates, J. A., Firbank, S. J., Lewis, R. J., Grondin, G. G., Ghinet, M. G., Gloster, T. M., Herve, C., Knox, J. P., Talbot, B. G., Turkenburg, J. P., Kerovuo, J., Brzezinski, R., Fontes, C. M. G. A., Davies, G. J., Boraston, A. B., and Gilbert, H. J. (2009) Evidence that family 35 carbohydrate binding modules display conserved specificity but divergent function. *Proc. Natl. Acad. Sci. U. S. A.* **106**, 3065–3070

17. Correia, M. A. S., Abbott, D. W., Gloster, T. M., Fernandes, V. O., Prates, J. A. M.,

514 Montanier, C., Dumon, C., Williamson, M. P., Tunnicliffe, R. B., Liu, Z., Flint, J. E.,
515 Davies, G. J., Henrissat, B., Coutinho, P. M., Fontes, C. M. G. A., and Gilbert, H. J.
516 (2010) Signature active site architectures illuminate the molecular basis for ligand
517 specificity in family 35 carbohydrate binding module. *Biochemistry*. **49**, 6193–6205
518 18. Couturier, M., Roussel, A., Rosengren, A., Leone, P., Stålbrand, H., and Berrin, J. G.
519 (2013) Structural and biochemical analyses of glycoside hydrolase families 5 and 26
520 β-(1,4)-mannanases from *Podospora anserina* reveal differences upon
521 manno-oligosaccharide catalysis. *J. Biol. Chem.* **288**, 14624–14635
522 19. Okazawa, Y., Miyazaki, T., Yokoi, G., Ishizaki, Y., Nishikawa, A., and Tonozuka, T.
523 (2015) Crystal structure and mutational analysis of isomaltodextranase, a member of
524 glycoside hydrolase family 27. *J. Biol. Chem.* **290**, 26339–26349
525 20. Fujimoto, Z., Kishine, N., Suzuki, N., Suzuki, R., Mizushima, D., Momma, M.,
526 Kimura, K., and Funane, K. (2017) Isomaltooligosaccharide-binding structure of
527 *Paenibacillus* sp. 598K cycloisomaltooligosaccharide glucanotransferase. *Biosci. Rep.*
528 **37**, 1–11
529 21. Suzuki, N., Fujimoto, Z., Kim, Y. M., Momma, M., Kishine, N., Suzuki, R., Suzuki, S.,
530 Kitamura, S., Kobayashi, M., Kimura, A., and Funane, K. (2014) Structural
531 Elucidation of the Cyclization Mechanism of α-1,6-Glucan by *Bacillus circulans*
532 T-3040 Cycloisomaltooligosaccharide Glucanotransferase. *J. Biol. Chem.* **289**, 12040–

12051

22. Light, S. H., Cahoon, L. A., Halavaty, A. S., Freitag, N. E., and Anderson, W. F. (2016) Structure to function of an α-glucan metabolic pathway that promotes *Listeria monocytogenes* pathogenesis. *Nat. Microbiol.* **2**, 1–10

23. Fujimoto, Z., Suzuki, N., Kishine, N., Ichinose, H., Momma, M., Kimura, A., and Funane, K. (2017) Carbohydrate-binding architecture of the multi-modular α-1,6-glucosyltransferase from *Paenibacillus* sp. 598K, which produces α-1,6-glucosyl-α-glucosaccharides from starch. *Biochem. J.* **474**, 2763–2778

24. Ji, S., Dix, S. R., Aziz, A. A., Sedelnikova, S. E., Baker, P. J., Rafferty, J. B., Bullough, P. A., Tzokov, S. B., Agirre, J., Li, F. L., and Rice, D. W. (2019) The molecular basis of endolytic activity of a multidomain alginate lyase from *Defluviitalea phaphyphila*, a representative of a new lyase family, PL39. *J. Biol. Chem.* **294**, 18077–18091

25. Mandelli, F., De Morais, M. A. B., De Lima, E. A., Oliveira, L., Persinoti, G. F., and Murakami, M. T. (2020) Spatially remote motifs cooperatively affect substrate preference of a ruminal GH26-type endo-β-1,4-mannanase. *J. Biol. Chem.* **295**, 5012–5021

26. Guillén, D., Sánchez, S., and Rodríguez-Sanoja, R. (2010) Carbohydrate-binding domains: Multiplicity of biological roles. *Appl. Microbiol. Biotechnol.* **85**, 1241–1249

27. Burnley Tom, B., Afonine, P. V., Adams, P. D., and Gros, P. (2012) Modelling

552 dynamics in protein crystal structures by ensemble refinement. *Elife*. **2012**, 1–29

553 28. Ichinose, H., Kuno, A., Kotake, T., Yoshida, M., Sakka, K., Hirabayashi, J.,

554 Tsumuraya, Y., and Kaneko, S. (2006) Characterization of an exo-β-1,3-galactanase

555 from *Clostridium thermocellum*. *Appl. Environ. Microbiol.* **72**, 3515–3523

556 29. Bianchetti, C. M., Takasuka, T. E., Deutsch, S., Udell, H. S., Yik, E. J., Bergeman, L.

557 F., and Fox, B. G. (2015) Active site and laminarin binding in glycoside hydrolase

558 family 55. *J. Biol. Chem.* **290**, 11819–11832

559 30. Ishida, T., Fushinobu, S., Kawai, R., Kitaoka, M., Igarashi, K., and Samejima, M.

560 (2009) Crystal Structure of Glycoside Hydrolase Family 55 β -1,3-Glucanase from the

561 Basidiomycete. *J. Biol. Chem.* **284**, 10100–10109

562 31. Karkehabadi, S., Helmich, K. E., Kaper, T., Hansson, H., Mikkelsen, N. E.,

563 Gudmundsson, M., Piens, K., Fujdala, M., Banerjee, G., Scott-Craig, J. S., Walton, J.

564 D., Phillips, G. N., and Sandgren, M. (2014) Biochemical characterization and crystal

565 structures of a fungal family 3 β-glucosidase, Cel3A from *Hypocrea jecorina*. *J. Biol.*

566 *Chem.* **289**, 31624–31637

567 32. Chandrasekaran, R., and Janaswamy, S. (2002) Morphology of western larch

568 arabinogalactan. *Carbohydr. Res.* **337**, 2211–2222

569 33. Kitazawa, K., Tryfona, T., Yoshimi, Y., Hayashi, Y., Kawauchi, S., Antonov, L.,

570 Tanaka, H., Takahashi, T., Kaneko, S., Dupree, P., Tsumuraya, Y., and Kotake, T.

(2013) β-galactosyl Yariv Reagent Binds To the β-1,3-Galactan of Arabinogalactan Proteins. *Plant Physiol.* **161**, 1117–1126

34. Otwinowski, Z., and Minor, W. (1997) Processing of X-ray diffraction data collected in oscillation mode. *Methods Enzymol.* **276**, 307–326

35. Terwilliger, T. C., and Berendzen, J. (1999) Automated MAD and MIR structure solution. *Acta Crystallogr. Sect. D Biol. Crystallogr.* **55**, 849–861

36. Perrakis, A., Morris, R., and Lamzin, V. S. (1999) Automated protein model building combined with iterative structure refinement. *Nat. Struct. Biol.* **6**, 458–463

37. Winn, M. D., Ballard, C. C., Cowtan, K. D., Dodson, E. J., Emsley, P., Evans, P. R., Keegan, R. M., Krissinel, E. B., Leslie, A. G. W., McCoy, A., McNicholas, S. J., Murshudov, G. N., Pannu, N. S., Potterton, E. A., Powell, H. R., Read, R. J., Vagin, A., and Wilson, K. S. (2011) Overview of the CCP4 suite and current developments. *Acta Crystallogr. Sect. D Biol. Crystallogr.* **67**, 235–242

38. Emsley, P., Lohkamp, B., Scott, W. G., and Cowtan, K. (2010) Features and development of Coot. *Acta Crystallogr. Sect. D Biol. Crystallogr.* **66**, 486–501

39. Murshudov, G. N., Vagin, A. A., and Dodson, E. J. (1997) Refinement of macromolecular structures by the maximum-likelihood method. *Acta Crystallogr. Sect. D Biol. Crystallogr.* **53**, 240–255

40. Afonine, P. V., Grosse-Kunstleve, R. W., Echols, N., Headd, J. J., Moriarty, N. W.,

590 Mustyakimov, M., Terwilliger, T. C., Urzhumtsev, A., Zwarta, P. H., and Adams, P. D.
591 (2012) Towards automated crystallographic structure refinement with phenix . refine
592 research papers. *Acta Crystallogr. - Sect. D Biol. Crystallogr.* **68**, 352–367
593 41. Burnley, B. T., and Gros, P. (2013) phenix.ensemble_refinement: a test study of apo
594 and holo BACE1. *Comput. Crystallogr. Newsl.* **4**, 51–58
595 42. Forneris, F., Burnley, B. T., and Gros, P. (2014) Ensemble refinement shows
596 conformational flexibility in crystal structures of human complement factor D. *Acta*
597 *Crystallogr. Sect. D Biol. Crystallogr.* **70**, 733–743
598 43. Liebschner, D., Afonine, P. V., Baker, M. L., Bunkoczi, G., Chen, V. B., Croll, T. I.,
599 Hintze, B., Hung, L. W., Jain, S., McCoy, A. J., Moriarty, N. W., Oeffner, R. D., Poon,
600 B. K., Prisant, M. G., Read, R. J., Richardson, J. S., Richardson, D. C., Sammito, M. D.,
601 Sobolev, O. V., Stockwell, D. H., Terwilliger, T. C., Urzhumtsev, A. G., Videau, L. L.,
602 Williams, C. J., and Adams, P. D. (2019) Macromolecular structure determination
603 using X-rays, neutrons and electrons: Recent developments in Phenix. *Acta Crystallogr.*
604 *Sect. D Struct. Biol.* **75**, 861–877
605 44. Vagin, A., and Teplyakov, A. (2010) Molecular replacement with MOLREP. *Acta*
606 *Crystallogr. Sect. D Biol. Crystallogr.* **66**, 22–25
607 45. Wallace, A. C., Laskowski, R. A., and Thornton, J. M. (1995) LIGPLOT: a program to
608 generate schematic diagrams of protein-ligand interactions The LIGPLOT program

automatically generates schematic 2-D representations of protein-ligand complexes from standard Protein Data Bank file input. *Protein Eng.* **8**, 127–134

46. Laskowski, R. A., and Swindells, M. B. (2011) LigPlot+: Multiple ligand-protein interaction diagrams for drug discovery. *J. Chem. Inf. Model.* **51**, 2778–2786

47. Ashkenazy, H., Erez, E., Martz, E., Pupko, T., and Ben-Tal, N. (2010) ConSurf 2010: Calculating evolutionary conservation in sequence and structure of proteins and nucleic acids. *Nucleic Acids Res.* **38**, 529–533

48. Landau, M., Mayrose, I., Rosenberg, Y., Glaser, F., Martz, E., Pupko, T., and Ben-Tal, N. (2005) ConSurf 2005: The projection of evolutionary conservation scores of residues on protein structures. *Nucleic Acids Res.* **33**, 299–302

49. Celniker, G., Nimrod, G., Ashkenazy, H., Glaser, F., Martz, E., Mayrose, I., Pupko, T., and Ben-Tal, N. (2013) ConSurf: Using evolutionary data to raise testable hypotheses about protein function. *Isr. J. Chem.* **53**, 199–206

50. Ashkenazy, H., Abadi, S., Martz, E., Chay, O., Mayrose, I., Pupko, T., and Ben-Tal, N. (2016) ConSurf 2016: an improved methodology to estimate and visualize evolutionary conservation in macromolecules. *Nucleic Acids Res.* **44**, W344–W350

51. Glaser, F., Pupko, T., Paz, I., Bell, R. E., Bechor-Shental, D., Martz, E., and Ben-Tal, N. (2003) ConSurf: Identification of functional regions in proteins by surface-mapping of phylogenetic information. *Bioinformatics*. **19**, 163–164

628 52. Korotkova, O. G., Semenova, M. V., Morozova, V. V., Zorov, I. N., Sokolova, L. M.,
629 Bubnova, T. M., Okunev, O. N., and Sinitsyn, A. P. (2009) Isolation and properties of
630 fungal β-glucosidases. *Biochem.* **74**, 569–577
631 53. Kumar, S., Stecher, G., Li, M., Knyaz, C., and Tamura, K. (2018) MEGA X:
632 Molecular evolutionary genetics analysis across computing platforms. *Mol. Biol. Evol.*
633 **35**, 1547–1549
634 54. Stecher, G., Tamura, K., and Kumar, S. (2020) Molecular evolutionary genetics
635 analysis (MEGA) for macOS. *Mol. Biol. Evol.* **37**, 1237–1239
636 55. Robert, X., and Gouet, P. (2014) Deciphering key features in protein structures with
637 the new ENDscript server. *Nucleic Acids Res.* **42**, 320–324
638 56. Bohne, A., Lang, E., and Von Der Lieth, C. W. Der (1998) W3-SWEET: Carbohydrate
639 modeling by internet. *J. Mol. Model.* **4**, 33–43
640 57. Bohne, A., Lang, E., and Von Der Lieth, C. W. (1999) SWEET - WWW-based rapid
641 3D construction of oligo- and polysaccharides. *Bioinformatics*. **15**, 767–768
642

643 Table 1. Data collection statistics

Data	WT	SeMet (peak)	(edge)	(low remote)	(high remote)	WT Gal3 soakir	E208Q Gal 3 co-cry	E208A Gal3 co-cry
Space group	*P*1	$P2_1$	$P2_1$	$P2_1$	$P2_1$	$P2_12_12_1$	$P2_1$	$P3_221$
Unit-cell parameters (Å, °)	*a*=40.5 *b*=66.3 *c*=74.0 α=72.0 β=84.7 γ=82.1	*a*=66.4 *b*=50.5 *c*=75.8 α=90.0 β=111.9 γ=90.0				*a*=50.8 *b*=66.6 *c*=106.4 α=90.0 β=90.0 γ=90.0	*a*=66.1 *b*=50.4, *c*=75.7 α=90.0 β=111.3 γ=90.0	*a*=156.7 *b*=156.7 *c*=147.7 α=90.0 β=120.0 γ=90.0
Beam Line	PF BL-5	PF BL-6A	PF BL-6A	PF BL-6A	PF BL-6A	PF-AR NW12	PF-AR NE3	PF-AR NE3
Detector	ADSC Q315	ADSC Q4R				ADSC Q210	ADSC Q270	ADSC Q270
Wavelength (Å)	0.90646	0.97882	0.97950	0.98300	0.96400	1.0000	1.0000	1.0000
Resolution (Å)	50-1.40 (1.45-1.40)	50.0-1.80 (1.86-1.80)	50.0-2.00 (2.07-2.00)	50.0-2.00 (2.07-2.00)	50.0-2.00 (2.07-2.00)	100.0-1.50 (1.55-1.50)	50.0-2.50 (2.54-2.50)	100.0-2.30 (2.38-2.30)
R_{sym}	0.054 (0.370)	0.079 (0.672)	0.061 (0.307)	0.060 (0.303)	0.062 (0.307)	0.046 (0.109)	0.143 (0.399)	0.167 (0.627)
Completeness (%)	95.6 (89.0)	100.0 (99.9)	100.0 (100.0)	100.0 (100.0)	100.0 (100.0)	97.5 (94.9)	96.2 (83.0)	99.1 (92.0)
Multiplicity	3.8 (3.1)	14.0 (12.6)	7.2 (6.9)	7.2 (6.9)	7.2 (7.0)	9.2 (8.9)	4.4 (3.0)	9.7 (5.1)
Average $I/\sigma(I)$	24.4 (2.8)	36.6 (4.7)	30.9 (8.3)	30.8 (8.2)	31.3 (8.2)	48.9 (21.0)	13.5 (2.7)	17.9 (2.7)
Unique reflections	136 692 (12 747)	43 643 (4 353)	31 744 (3 139)	31 760 (3 144)	31 780 (3 146)	57 278 (5 493)	16 007 (702)	92 497 (8 510)
Observed reflections	520 085	613 162	227 158	228 381	228 595	524 957	69 939	900 469
Z	2	1				1	1	4

644

645 Table 2. Refinement statistics

Data	WT	WT_Gal	E208Q_Gal3	E208A_Gal3
Resolution range	7.997 - 1.398 (1.448 - 1.398)	41.56 - 1.500 (1.554 - 1.500)	29.79 - 2.499 (2.588 - 2.499)	30.66 - 2.300 (2.382 - 2.300)
Completeness (%)	95.46 (87.82)	97.51 (94.80)	96.41 (85.67)	98.78 (92.17)
Wilson B-factor	12.76	10.11	29.91	30.40
Reflections used in refinement	136655 (12497)	57105 (5474)	15762 (1381)	92011 (8507)
Reflections used for R-free	6862 (630)	2884 (272)	799 (64)	4568 (441)
R-work (%)	15.47 (22.50)	13.43 (12.71)	16.62 (25.54)	16.10 (22.39)
R-free (%)	18.56 (26.28)	16.00 (17.93)	24.39 (42.53)	21.43 (28.28)
Number of non-hydrogen atoms	7966	3923	3576	14570
macromolecules	6615	3290	3235	12886
ligands	109	121	114	678
solvent	1242	512	227	1006
Protein residues	2106	427	428	1708
RMS (bonds)	0.008	0.006	0.008	0.011
RMS (angles)	1.22	0.87	0.94	1.05
Ramachandran favored (%)	97.29	97.41	94.13	95.76
Ramachandran allowed (%)	2.71	2.59	5.87	4.24
Ramachandran outliers (%)	0	0	0	0
Rotamer outliers (%)	0.81	0.55	0.29	0.36
Clash score	2.06	1.95	6.94	3.50
Average B-factor (Å^2)	17.21	12.45	30.48	32.98
macromolecules	14.97	10.57	29.77	31.60
ligands	29.38	23.33	52.26	56.11
solvent	28.09	22.02	29.74	35.03
PDB ID	7BYS	7BYT	7BYV	7BYX

646

647 Table 3. Refinement statistics of ensemble refinement

Data	WT	WT_Gal	E208Q_Gal3	E208A_Gal3
Resolution range	7.997-1.398 (1.448-1.398)	41.56-1.500 (1.554-1.500)	29.79-2.499 (2.588-2.499)	30.66-2.300 (2.382- 2.300)
Completeness (%)	95.97(82)	97.52 (95)	96.47 (88)	98.93(87)
pTLS (%)	0.9	0.9	0.9	1.0
Tx	1.0	0.9	0.3	0.4
Wilson B-factor	12.8	10.1	29.9	30.4
Reflections used in refinement	136649	57112	15759	91994
Reflections used for R-free	6862	2885	799	4569
R-work	13.81 (24.36)	12.08 (10.68)	17.82 (24.73)	15.92 (22.56)
R-free	17.08 (26.30)	15.29 (17.10)	23.33 (32.75)	20.71 (28.84)
RMS(bonds)	0.008	0.010	0.007	0.008
RMS(angles)	1.171	1.312	1.078	1.090
Ramachandran favored (%)	94.06	95.39	88.98	92.62
Ramachandran allowed (%)	5.08	4.03	9.19	7.24
Ramachandran outliers (%)	0.86	0.58	1.83	0.74
Rotamer outliers (%)	7.45	7.00	11.05	7.85
Clash score	0	0	0	0
Average B-factor (Å2)	13.65	9.55	28.32	32.83
macromolecules	13.63	9.54	28.30	32.66
ligands	14.97	9.82	28.98	36.05
Molprobity score	1.56	1.45	1.87	1.64
model number	100	103	20	34

648

649

650 **Figure legends**

651 Fig. 1. Overall structure of *Pc*1,3Gal43A. In the three-dimensional structure of *Pc*1,3Gal43A,
652 the five blades of the catalytic domain are shown in blue (Gln21-Leu87), cyan
653 (Ser88-Asp155), green (Ser156-Gly204), yellow (Ala205-Ser247), and orange
654 (Ala248-Asp297) with successive roman numerals. The CBM (The326-Val448) is shown in
655 orange. The linker connecting the two domains (Phe298-Gly325) is shown in gray.

656

657 Fig. 2. Gal3 binding mode at the catalytic site.
658 A: The surface structure of the catalytic center. Gal3 is represented as green (carbon) and red
659 (oxygen) sticks. B: Schematic diagram showing the interaction mode at the catalytic center.
660 Black, red, and blue show carbon, oxygen, and nitrogen, respectively. Red lines indicate the
661 hydrophobically interacting residues. This diagram was drawn with LigPlot+ (version 1.4.5).
662 C: The 2Fo-Fc omit map is drawn as a blue mesh (0.8 sigma). Residues are shown in white
663 (carbon), red (oxygen), and blue (nitrogen). Gal3 is shown in green (carbon) and red (oxygen).
664 Yellow dots indicate hydrogen bonds and/or hydrophobic interaction and red spheres show
665 water molecules interacting with ligands or residues.

666

667 Fig. 3. Surface structures of the CBM.

668 A: Substrate binding mode at CBM35. Green, cyan, magenta, and yellow indicate carbons of
669 chains A, B, C, and D of E208A_Gal3, respectively, and red shows oxygen. The left side is
670 the non-reducing end of Gal3, and the right side is the reducing end. B: calcium ion binding
671 mode at CBM35. Calcium ion is represented as green spheres and interacting residues are
672 shown as stick models. Yellow dots indicate interaction.
673
674 Fig. 4. Ligand interaction mode at CBM35.
675 A and E, B and F, C and G, and D and H are chains A, B, C, and D of E208A, respectively.
676 A to D: Interaction modes between ligand and CBM35 residues. Atoms are indicated in the
677 same colors as in Fig. 2. E to G: Schematic diagram showing the interaction mode at CBM35.
678 Atoms are indicated in the same colors as in Fig. 2. Sugar binding sites are named Gal_site 1,
679 Gal_site 2, and Gal_site 3 from the non-reducing end of the sugar, and in this figure, they are
680 labeled 1, 2, and 3, respectively.
681
682 Fig. 5. Results of ensemble refinement at the catalytic site.
683 Each model is divided into three parts for clarity. A (E, I), B (F, J), C (G, K), and D (H, L)
684 show WT, WT_Gal, E208Q_Gal3, and E208A_Gal3, respectively. Although WT and
685 E208A_Gal3 contained multiple molecules in an asymmetric unit, the results obtained with
686 multiple molecules were considered as an ensemble of one molecule in the present study.

687 Letters indicate the chain names. Atoms are indicated in the same colors as Fig. 2. Gal3 of the
688 structure of E208Q_Gal3 obtained by X-ray crystallography is arranged in each figure to
689 maximize ease of comparison.
690
691 Fig. 6. Results of ensemble refinement at the CBM ligand-binding site.
692 A,B, C, and D: Residues related to ligand interaction. In this figure, Gal3 of chain A of
693 refined E208A_Gal3 is drawn for comparison. E, F, G, and H: the ligands of each chain.
694 Green, cyan, and yellow are used in order from the non-reducing terminal Gal. A and E, B and
695 F, C and G, D and H represent chain A, B, C, and D of E208A_Gal3, respectively. Atoms are
696 indicated in the same colors as Fig. 2.
697
698 Fig. 7. Ligand conformation of ensemble refinement at glance. A: ligand conformation of
699 E208Q_Gal3 ensemble model. B: ligand conformation of E208A_Gal3 ensemble models with
700 four chains aligned. Green, cyan, and yellow are used in order from the non-reducing terminal
701 Gal.
702
703 Fig. 8. Catalytic domain structure comparison. A: Visualization of the degree of preservation
704 of GH43_sub24. The degree of conservation of amino acid residues in the catalytic domain of
705 GH43_sub24 was visualized using the ConSurf server (https://consurf.tau.ac.il), the query for

706 BLAST was set to *Pc*1,3Gal43A, and the conservation degree was analyzed based on 150
707 amino acid sequences in the ConSurf server (47–51). The conservation degree is shown in
708 graded color. Preservation degrees are shown in a gradient with cyan for the lowest degree of
709 preservation and blue for the highest. B: Catalytic domain comparison of *Pc*1,3Gal43A and
710 two GH43_sub24 galactanases. Catalytic center of E208Q_Gal3 of *Pc*1,3Gal43A (white, PDB
711 ID: 7BYV), BT3683 (cyan, PDB ID: 6EUI), and *Ct*1,3Gal43A (pink, PDB ID: 3VSF). Red,
712 blue, and yellow represent oxygen atoms, nitrogen atoms, and sulfur atoms, respectively.
713 Residue names mean *Pc*1,3Gal43A/ BT3683/ *Ct*1,3Gal43A.
714
715 Fig. 9. Structure comparison of the catalytic sites of *Pc*1,3Gal43A (A), GH55
716 exo-β-1,3-glucanase from *P. chrysosporium* (B; *Pc*Lam55A; PDB ID: 3EQO), GH55
717 exo-β-1,3-glucanase from *Streptomyces* sp. SirexAA-E (C; SacteLam55A; PDB ID 4PF0),
718 GH3 β-glucosidase from *H. jecorina* (C, PDB ID: 3ZYZ).
719 A, B, and C hydrolyze the main chain of β-1,3-galactan or β-1,3-glucan, bypassing
720 β-1,6-branched side chains (6, 29, 30). D hydrolyzes four types of β-bonds, and it does not
721 bypass side chains (31, 52). The upper panel shows the overall surface structure and the lower
722 panel shows an enlarged view of the catalytic region. Orange dashed circles indicate the space
723 near the C-6 position of Gal or glucose at the non-reducing end.
724

725 Figure. 10. Sequence alignment of known CBM35s (A) and structure comparison between
726 CBM35s of *Pc*1,3Gal43A (B) and Cte_2137 (C).
727 A: Taxon names are shown as scientific names, ligand specificity and PDB ID only for brevity.
728 When the same enzyme contains two CBM35 domains, the taxon name is indicated with 1 on
729 the N-terminal and 2 on the C-terminal. Gal, Glc, Man, Xyl, and Uronic means ligand
730 specificities for Gal, glucose, mannose, xylose, and glucronic acid and/or galacturonic acid,
731 respectively. Among these, 3ZM8, 6UEH, and 2BGO, which bind to Man, are Type B CBMs,
732 which show endo-type binding, while the other 14 are all Type C CBMs, which show
733 exo-type binding. The alignment was built by using MUSCLE on MEGAX: Molecular
734 Evolutionary Genetics Analysis (53, 54), and the figure was generated with ESPrint
735 3.0 (http://espript.ibcp.fr; 56). Orange and green boxes represent ligand binding and calcium
736 ion binding residues, respectively. B and C: Ligand binding residues of *Pc*1,3Gal43A (chain A
737 of E208A_Gal3) and Cte_2137 (PDB ID: 2WZ8). Red and blue mean oxygen and nitrogen,
738 respectively. The green stick model represents Gal3.
739
740 Table titles
741 Table 1. Data collection statistics
742 Table 2. Refinement statistics
743 Table 3. Refinement statistics of ensemble refinement
744

745 Fig. 1.

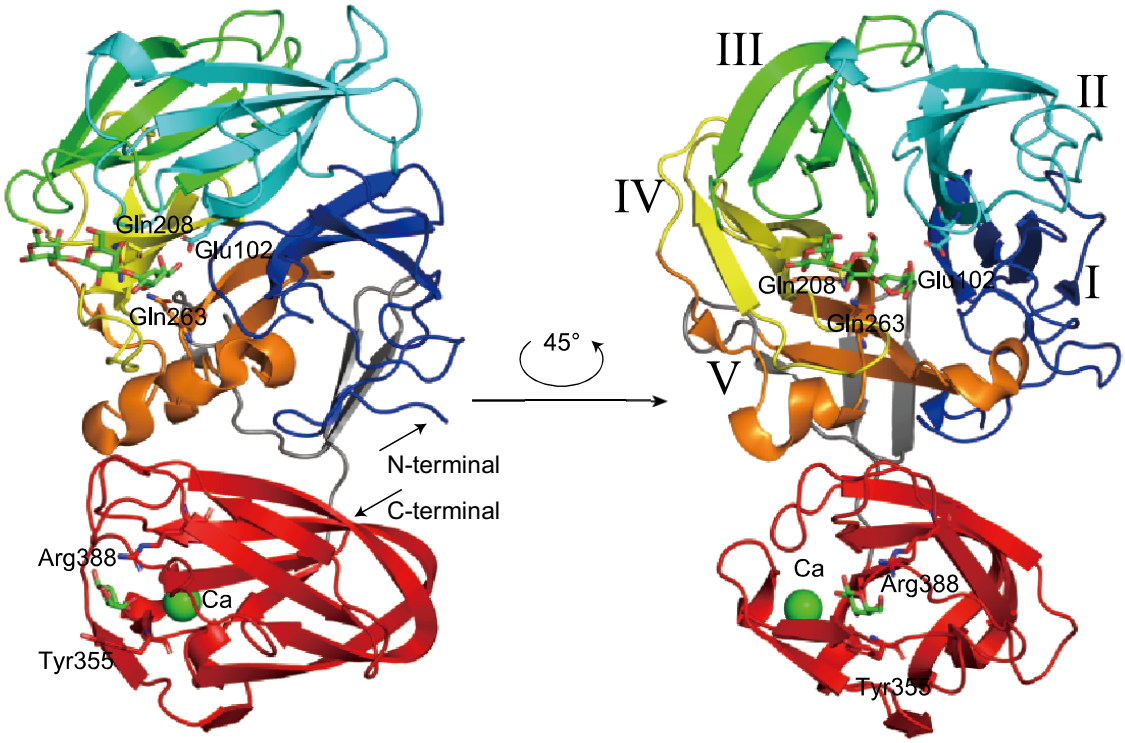

746

747

748

749 Fig. 2.

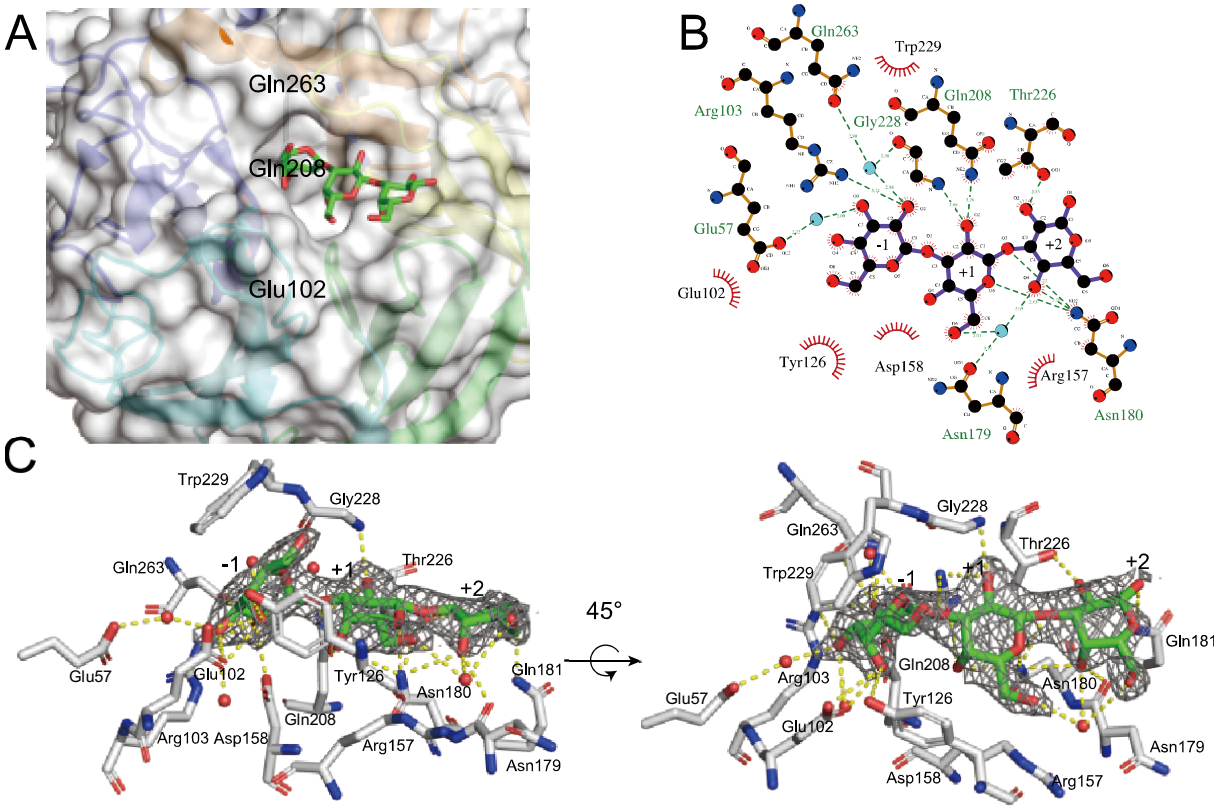

750
751

752 Fig. 3.

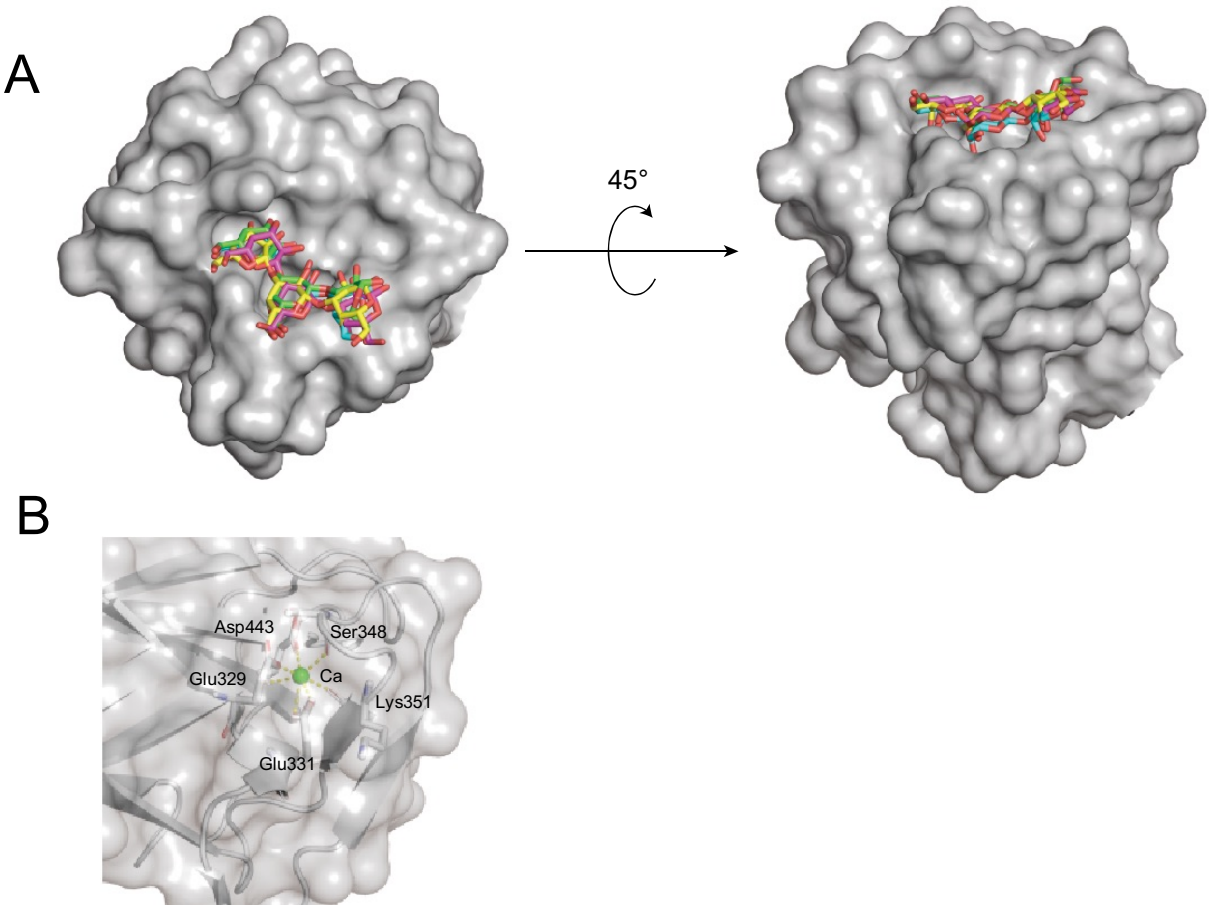

753

754

755 Fig. 4.

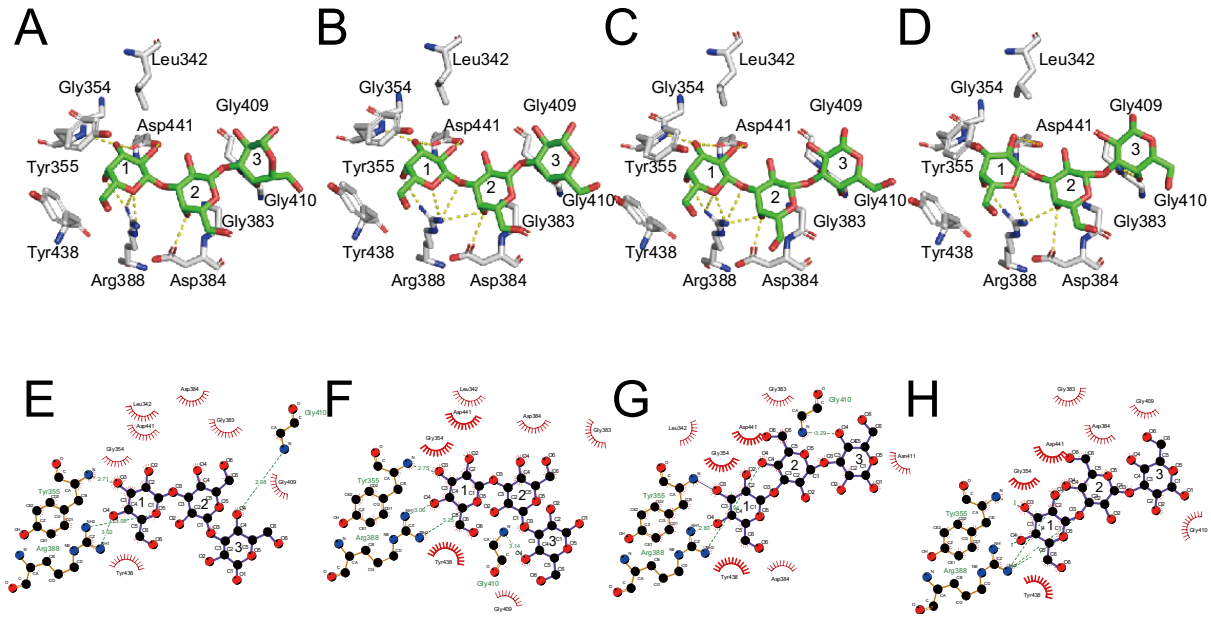

756

757

758 Fig. 5

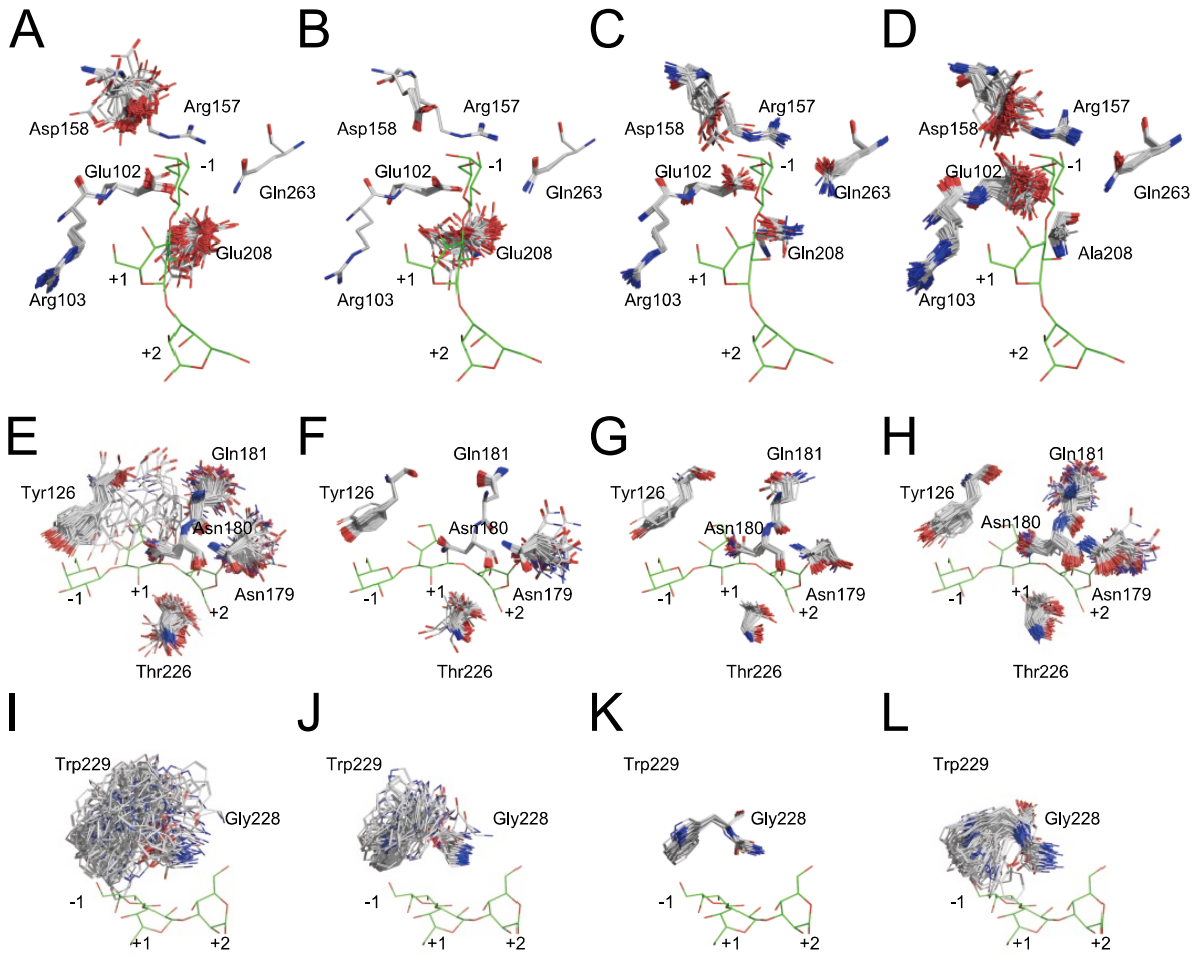

759

760

761 Fig. 6.

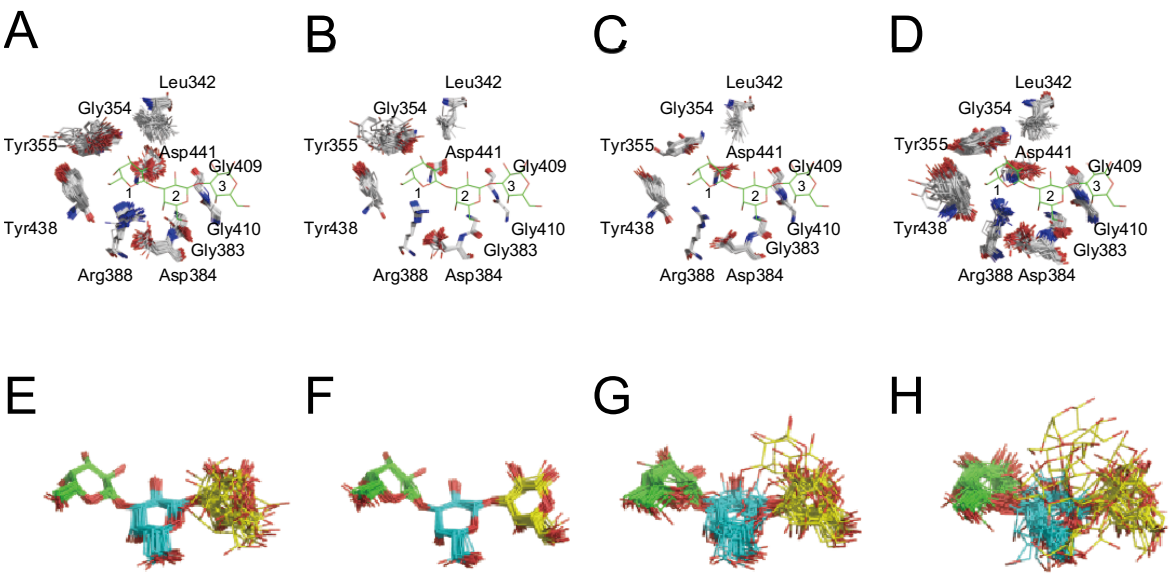

762

763

764 Fig. 7.

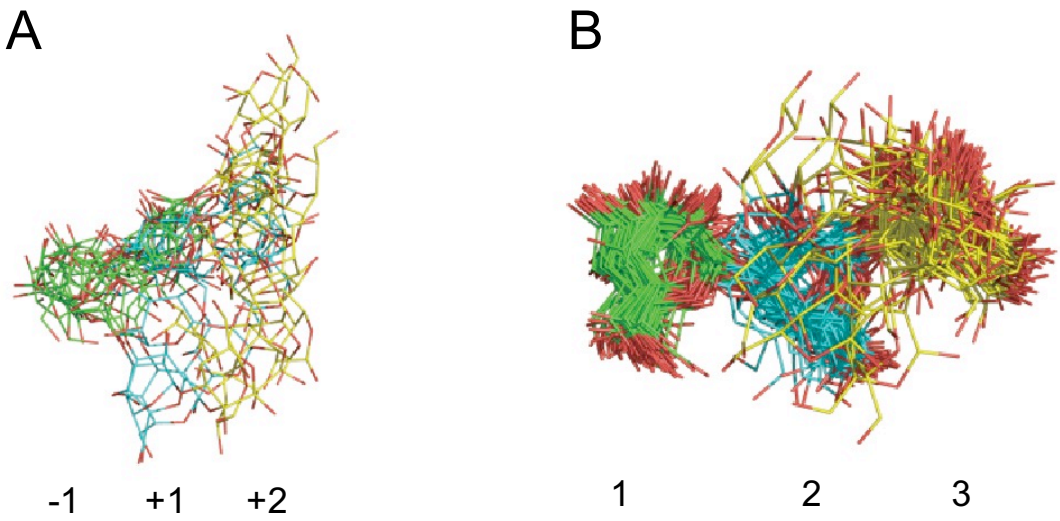

765

766

767 Fig. 8.

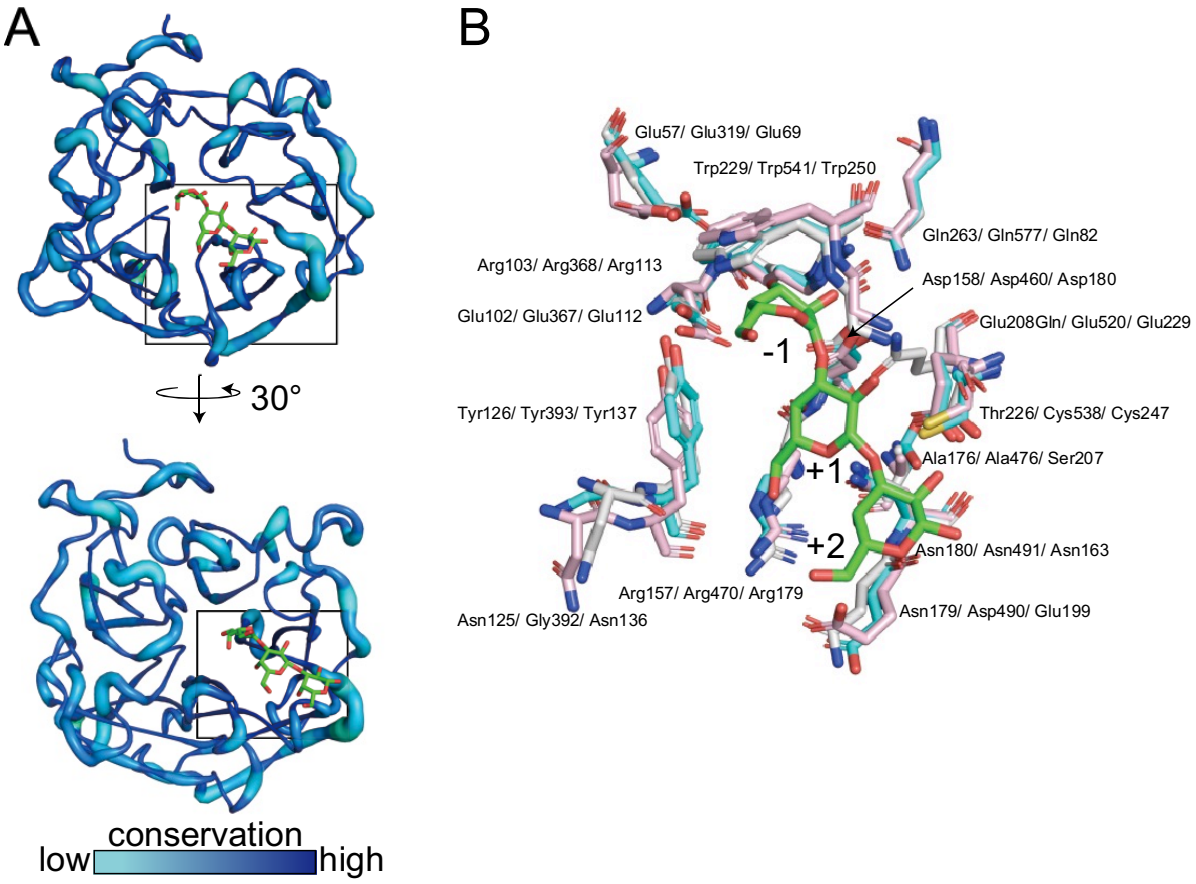

768

769

770

771 Fig. 9.

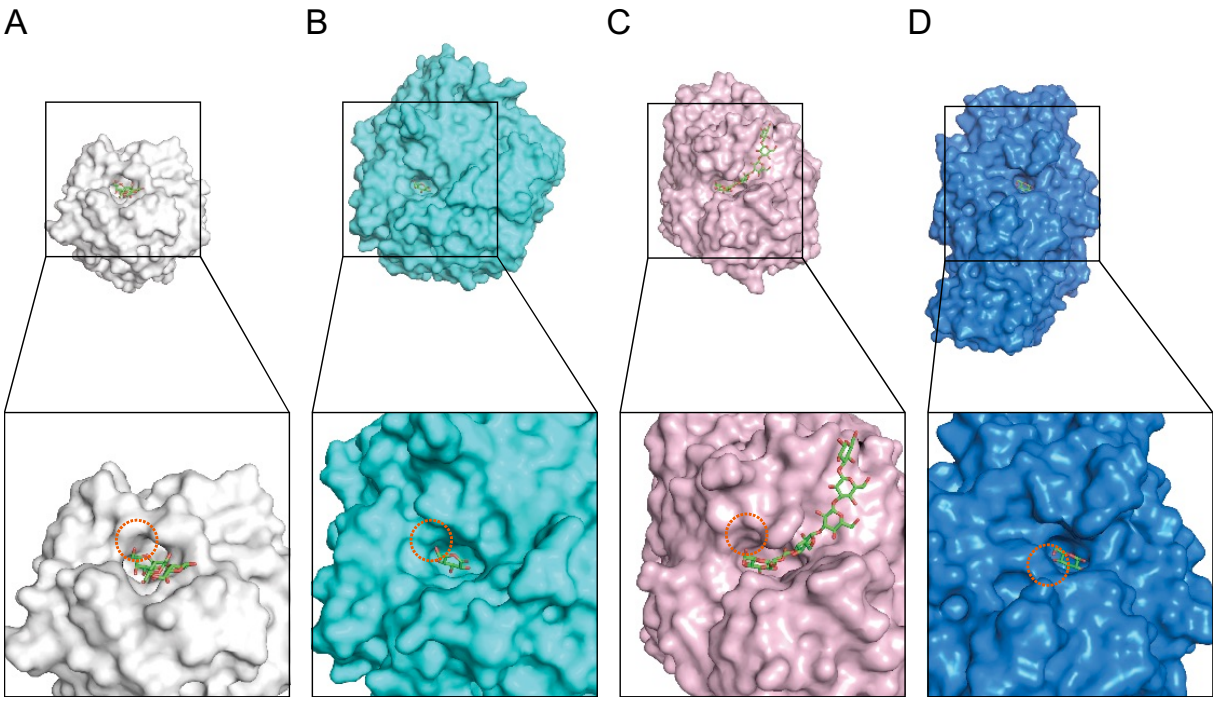

772

773

774 Fig. 10.

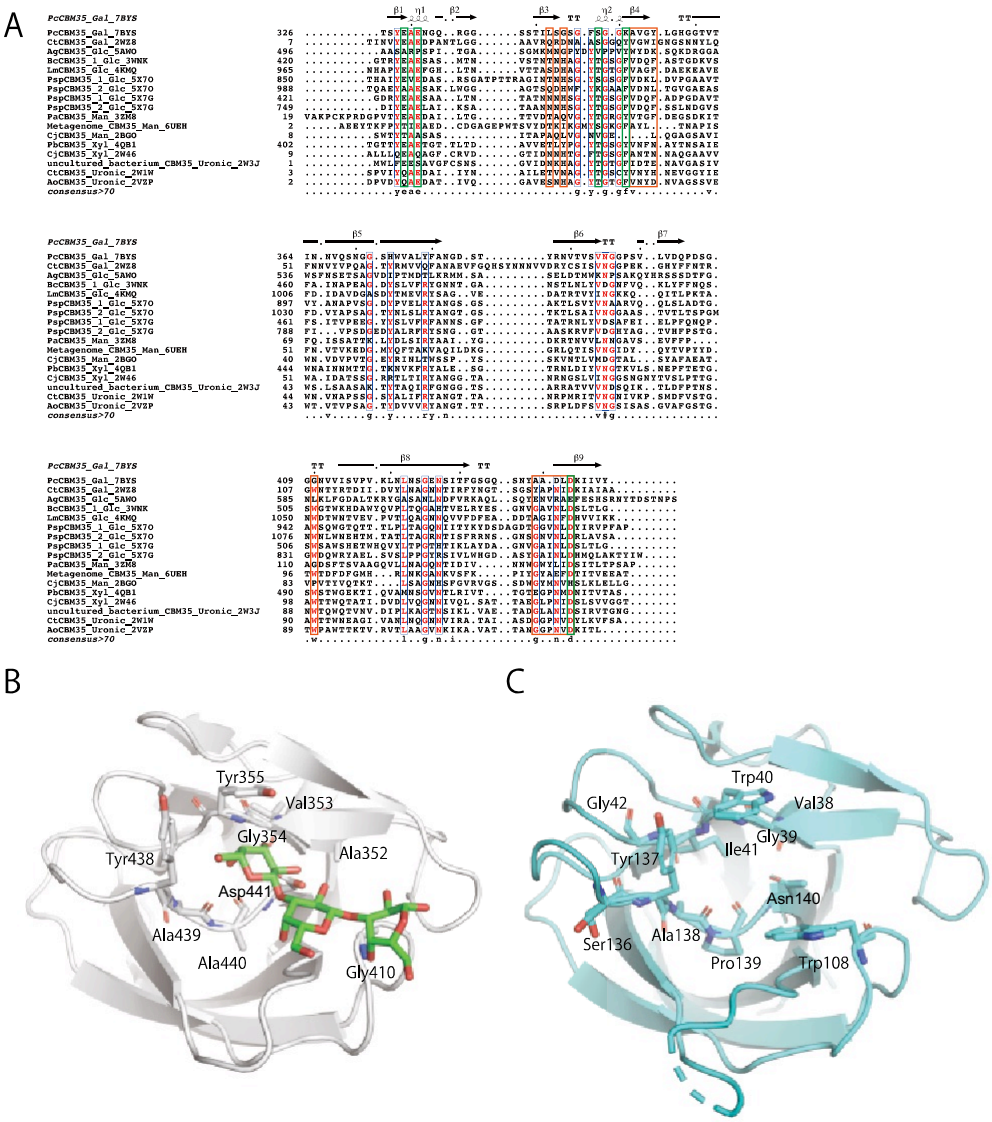

775